





Optimization of AC–DC Converters for Regenerative Train Suspensions

Luigi Costanzo , Alessandro Lo Schiavo , *Senior Member, IEEE*, Massimo Vitelli , and Lei Zuo 

Abstract—This article focuses on the dynamic optimization of the operating conditions of two types of ac–dc converters, a diode bridge rectifier and a full bridge active rectifier, which are used for interfacing regenerative rail vehicle suspensions based on ac electromagnetic generators. A theoretical analysis shows that, for both types of converters, the optimal operating conditions, leading to the maximization of the extracted power, can be predicted from the measurement of the generator speed. In particular, as regards the diode bridge rectifier, it is shown that the optimal value of the dc side voltage is related to the generator speed. As regards the active full-bridge rectifier, it is shown that a relationship exists between the optimal converter duty cycle and the generator speed. Experimental results validate the proposed theoretical models both in case of ideal constant generator speeds, and in case of more realistic time-variable generator speeds. The proposed analysis enables the design of high-performance speed-driven maximum power point tracking techniques for regenerative vehicle suspensions.

Index Terms—AC–DC converter, maximum power point tracking, power optimization, regenerative train suspension.

I. INTRODUCTION

ON BOARD sensors used for continuous monitoring or tracking of freight railcars need energy supply for measuring and for transmitting information. The lack of electricity in freight cars can be overcome by resorting to the harvesting of wasted energy [1]–[3]. In particular, regenerative suspensions are aimed at the harvesting of the vibrations' mechanical energy otherwise dissipated in traditional railcar suspensions. Different regenerative suspensions have been proposed in literature and the great majority of them exploit an electromagnetic generator to convert the mechanical energy into electrical energy [4].

Manuscript received May 26, 2021; revised September 21, 2021; accepted November 18, 2021. Date of publication December 16, 2021; date of current version March 20, 2022. Paper 2021-TSC-0583.R1, presented at the IEEE 20th Mediterranean Electrotechnical Conference, Palermo, Italy, Jun. 16–18, 2020, and approved for publication in the IEEE TRANSACTIONS ON INDUSTRY APPLICATIONS by the Transportation Systems Committee of the IEEE Industry Applications Society. This work was partially supported by the “VALERE: VANviteLLi pER la RicERca” research program by Università degli Studi della Campania “Luigi Vanvitelli”. The work of L. Zuo was supported by the U.S. National Science Foundation under Grant IUCRC #1738689. (*Corresponding author: Luigi Costanzo.*)

Luigi Costanzo, Alessandro Lo Schiavo, and Massimo Vitelli are with the Department of Engineering, Università degli Studi della Campania “Luigi Vanvitelli,” 81031 Aversa CE, Italy (e-mail: luigi.costanzo@unicampania.it; alessandro.loschiavo@unicampania.it; massimo.vitelli@unicampania.it).

Lei Zuo is with the Center for Energy Harvesting Materials and Systems, Virginia Tech, Blacksburg, VA 24061 USA (e-mail: leizuo@vt.edu).

Color versions of one or more figures in this article are available at <https://doi.org/10.1109/TIA.2021.3136145>.

Digital Object Identifier 10.1109/TIA.2021.3136145

In energy harvesting applications, the most exploited ac–dc converter, to rectify the ac voltages produced by the electrical generators, is the diode bridge rectifier for its simplicity and low losses [5]. As the extracted power at the rectifier output is a function of the value of the dc side voltage [6]–[8], an optimal value of this voltage exists leading to the maximum power extraction, and such a value changes when the input vibrations characteristics vary with time. Since the maximization of the power extraction is crucial for energy harvesting systems, dynamic adaptations of the dc side voltage have been proposed to maximize the power generation [9]–[12]. In [13], it was shown that in a regenerative train suspension the value of the dc voltage at the output of the diode bridge rectifier that maximizes the average extracted power, is proportional to the generator speed. In [14], by exploiting the abovementioned result, an electronic interface based on the dynamic prediction of the maximum power point (MPP) starting from the measurement of the generator speed was designed.

This article extends the results in [13] and [14] by presenting an improved model for the relationship between the optimal value of the dc voltage of the diode bridge rectifier and the generator speed, which takes into account the diode voltage drops too, in order to increase the power extraction performance. Moreover, the results in [13] and [14] are here extended to active ac–dc converters by demonstrating that, also for such converters, the maximum power point can be predicted starting from the measurement of the generator speed. These converters allow better power extraction performances with respect to passive rectifiers due to their ability to manage not only the active power but also the reactive one. However, they are also characterized by more complex control techniques, which lead to higher control losses with respect to passive rectifiers. Hence, active ac–dc converters can become viable and very performing solutions only when low power management techniques are applied [15]–[17].

The rest of the article is organized as it follows. In Section II, the attention is focused on passive diode bridge rectifiers and a new speed-voltage model for the estimation of the optimal dc side voltage on the basis of the generator speed measurement is proposed. In Section III, the abovementioned considerations are extended to the case of an active full bridge rectifier and, in particular, it is shown that the optimal duty cycle of the full bridge switches can be obtained once the generator speed is measured. In Section IV, experimental results aimed at validating the theoretical analysis are reported. Finally, Section V concludes this article.

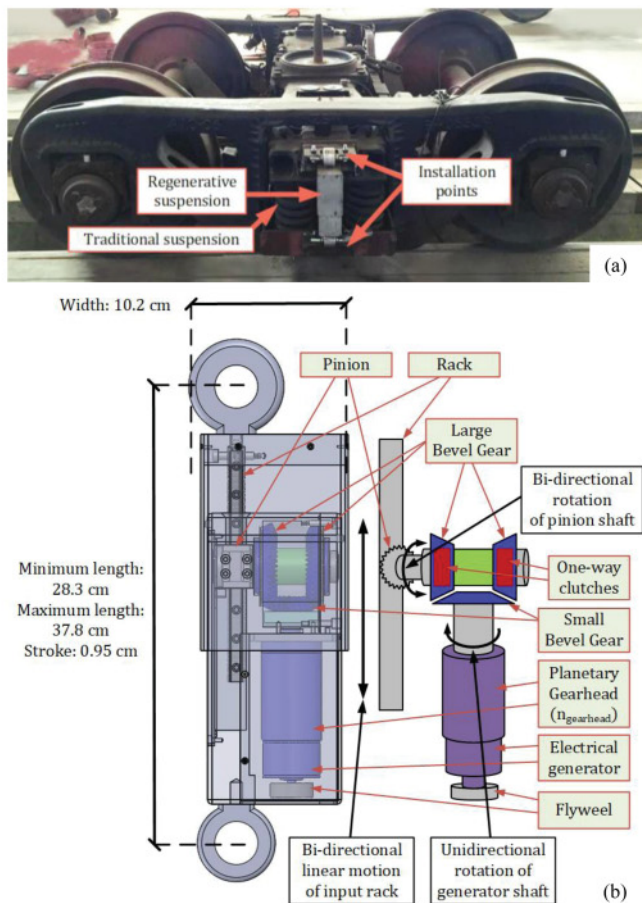


Fig. 1. (a) Onboard installation of a regenerative railcar suspension. (b) Schematic representation and block diagram.

II. PASSIVE AC-DC CONVERTER

A regenerative train suspension is able to convert the otherwise wasted mechanical energy of a train suspension into electrical energy. Such energy is associated to the vertical vibration of the wheel axle with respect to the bogie. In the considered regenerative train suspension shown in Fig. 1, the up and down displacement between the wheel axle and the bogie of the train is converted by the rack and the pinion into a bidirectional rotation and, then, into a unidirectional rotation by a mechanical motion rectifier (MMR) gearbox [18]. The unidirectional rotating shaft, whose speed is increased by a planetary gearhead, drives a flywheel and a three-phase electromagnetic generator. This is a three-phase brushless generator with Hall sensors by Maxon Group (model EC-i 40, number 496652 [21]), whose main mechanical and electrical characteristics are reported in Table I. The function of each mechanical component in the considered regenerative train suspension and the details of its operation are deeply investigated in [13], [14], and [18]–[20]. The power that can be extracted from the considered MMR-based regenerative suspension when applied to a freight railcar running on an operational track for different train speeds has been numerically and experimentally studied in [18].

TABLE I
MAIN MECHANICAL AND ELECTRICAL CHARACTERISTICS OF CONSIDERED REGENERATIVE TRAIN SUSPENSION

Symbol	Parameter	Value
J	Generator Rotary inertia	30 kg·cm ²
B	Generator Damping Coefficient	0.15 mNm/rpm
k_e	Generator Voltage Constant	0.0028 V/rpm
n_p	Number of Generator Pair Poles	7
R_{gen}	Generator Internal Resistance	0.72 Ω
L_{gen}	Generator Internal Inductance	0.57 mH
P_{gen}	Rated Power	50 W

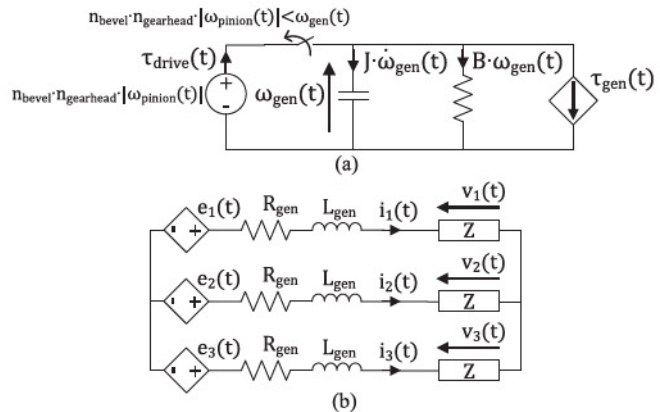


Fig. 2. (a) Equivalent circuit of the regenerative railcar suspension mechanical subsystem operating in both engagement mode (switch closed) and disengagement mode (switch open). (b) Equivalent circuit of the regenerative railcar suspension electrical subsystem.

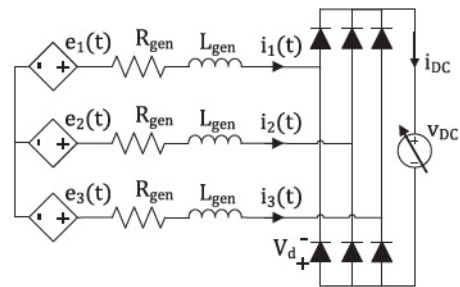


Fig. 3. Equivalent circuit of the regenerative train suspension electrical subsystem loaded by a diode bridge rectifier.

The equivalent circuits of the mechanical and of the electrical subsystems of the regenerative train suspension are reported in Fig. 2. ω_{gen} is the speed of the generator shaft, ω_{pinion} is the speed of the pinion shaft, n_{bevel} is the bevel gears ratio, $n_{gearhead}$ is the gearhead ratio, τ_{drive} is the external driving torque, B is the rotary damping coefficient, J is the rotary inertia, τ_{gen} is the resistive torque induced by the electrical generator, e_1 , e_2 , and e_3 are the induced voltages in the generator three phases, i_1 , i_2 , and i_3 are the currents flowing in such phases, v_1 , v_2 , and v_3 are the phase voltages across a wye connected load, R_{gen} and L_{gen} , respectively, are the resistance and inductance of the generator's phase coils, Z is a generic load. In Fig. 3, the generic load is replaced by a diode bridge rectifier.

A. Proportional Model for $v_{DC_MPP}(\omega_{gen})$

The value of the voltage v_{DC} at the dc side of the diode bridge rectifier that is able to extract the maximum average power from the regenerative train suspension, was identified in [13] and [14]. For a constant generator speed ω_{gen} , the induced voltages, e_1 , e_2 , and e_3 , are purely sinusoidal and, by neglecting the generator's phase coils inductance L_{gen} and the diodes voltage drops V_d , the average power at the output of the bridge rectifier can be written as a function of v_{DC} . In particular, as it is shown in details in the Appendix, the instantaneous power can be approximated as

$$p_{DC}(t) = \frac{\sqrt{3}k_e\omega_{gen} \cos(n_p \cdot \omega_{gen} \cdot t) \cdot v_{DC} - v_{DC}^2}{2 \cdot R_{gen}} \quad (1)$$

with $t \in [-\pi/(6 \cdot n_p \cdot \omega_{gen}), \pi/(6 \cdot n_p \cdot \omega_{gen})]$, k_e the generator voltage constant, n_p the number of generator pair poles, and R_{gen} the resistance of the generator's phase coils.

Equation (1) allows us to deduce the average power

$$P_{DC} = \frac{3\sqrt{3} \cdot k_e \cdot \omega_{gen} \cdot v_{DC}}{2 \cdot \pi \cdot R_{gen}} - \frac{v_{DC}^2}{2 \cdot R_{gen}}. \quad (2)$$

By differentiating (2) with respect to v_{DC} and by equating to zero the obtained expression, it is possible to calculate the optimal value v_{DC_MPP} of v_{DC} that maximizes P_{DC}

$$v_{DC_MPP} = \frac{3\sqrt{3}}{2\pi} \cdot k_e \cdot \omega_{gen} = m_{MPP} \cdot \omega_{gen}. \quad (3)$$

Equation (3) clearly highlights that the optimal dc-side voltage v_{DC_MPP} is proportional to the generator speed ω_{gen} .

The results of simulations performed in SPICE environment of the regenerative suspension with the parameters in Table I, are reported in Fig. 4. They show (point markers) the optimal value v_{DC_MPP} as a function of ω_{gen} for various values of the ratio L_{gen}/R_{gen} and of the diodes' voltage drops V_d . Such results are compared with the analytical results for v_{DC_MPP} obtained by (3) (dashed lines). The comparison shows that the ratio L_{gen}/R_{gen} has a negligible impact on the value of the optimal dc voltage whereas the effect of V_d on v_{DC_MPP} is not negligible at all.

Thus, the proportional model given by (3) can be improved by taking into account the effect of V_d .

B. Improved Model for $v_{DC_MPP}(\omega_{gen})$

If the diodes voltage drops V_d are not neglected, the instantaneous power can be written as

$$p_{DC}(t) = \frac{\sqrt{3}k_e\omega_{gen} \cos(n_p \cdot \omega_{gen} \cdot t) \cdot v_{DC}}{2 \cdot R_{gen}} - \frac{(v_{DC} + 2V_d) \cdot v_{DC}}{2 \cdot R_{gen}}. \quad (4)$$

By averaging (4), it is possible to obtain the average power delivered at the output of the diode bridge rectifier

$$P_{DC} = \frac{3\sqrt{3} \cdot k_e \cdot \omega_{gen} \cdot v_{DC}}{2 \cdot \pi \cdot R_{gen}} - \frac{(v_{DC} + 2V_d) \cdot v_{DC}}{2 \cdot R_{gen}}. \quad (5)$$

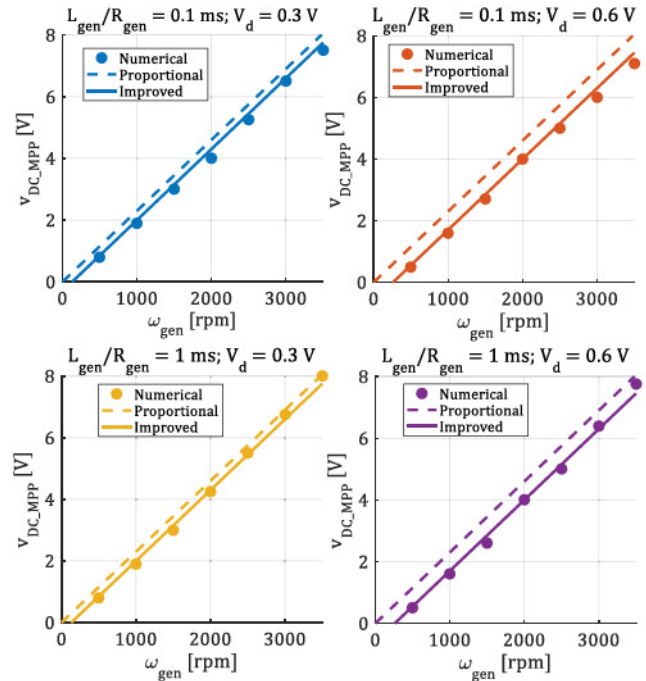


Fig. 4. Numerical and analytical results of the optimal value v_{DC_MPP} as a function of ω_{gen} , for various values of the ratio L_{gen}/R_{gen} (obtained by fixing $R_{gen} = 0.72 \Omega$ and by changing L_{gen} accordingly) and of the diodes voltage drops V_d .

Moreover, by differentiating (5) with respect to v_{DC} and by equating to zero the obtained expression, it is possible to find the new value of v_{DC_MPP}

$$v_{DC_MPP} = \frac{3\sqrt{3}}{2\pi} \cdot k_e \cdot \omega_{gen} - V_d = m_{MPP} \cdot \omega_{gen} + q_{MPP}. \quad (6)$$

Expression (6) provides an estimation of the optimal voltage at the dc-side of the diode bridge rectifier more accurate than (3), as it is shown in Fig. (4) (continuous lines). Experimental results reported in Section IV validates this more accurate model in presence of both constant and time-variable generator speeds.

The models in (3) or in (6) can be used to generate the reference signal for a controller of the dc-side rectifier voltage employed to maximize the power extraction. The reference signal can be generated in an open loop, in a closed loop or in a combined mode.

If the reference signal is generated in an open loop, i.e., by using theoretical models only, the whole control system is very fast, even if not very robust depending on system model and parameters. Thus, performances are improved by using the more accurate model in (6) instead of that in (3).

As an alternative to the open loop scheme, in order to cope with tolerances and time variability of system parameters, the reference signal can be generated by exploiting a feedback loop of the extracted power. This is the approach of the ‘‘Hill Climbing’’ techniques, which are typically employed in energy harvesting applications. They try to find the peak of the hill (the MPP) in a blind way, i.e., without any global information on the system, just exploiting the local information on the extracted

power. Thus, such kind of algorithms must operate step-by-step and take a time to reach the MPP. This can be not acceptable in applications with quickly time-varying MPPs, as it happens in regenerative suspensions due to the time variability of train suspension vibrations.

A further alternative to previous schemes, aimed at a fast and a robust response, is based on the combined action of a feedforward (open loop) prediction based on theoretical models and a feedback (closed) loop of the extracted power. The addition of a feedforward prediction to a feedback loop allows a significant increase of the dynamical performances of the whole system, with a dramatic reduction of the response time. The performance of a combined action of a feedforward prediction [based on the theoretical model (3)] and of an adaptive feedback loop was compared in [14] to that of a feedback loop based only on the widely used Perturb and Observe technique. It was experimentally demonstrated the advantage of the combined approach in regenerative suspension applications [14]. As well known, in the combined mode, the higher the accuracy of the model, the better the performance of the system. Thus, the more accurate model (6) allows a performance enhancement with respect to model (3).

III. ACTIVE AC–DC CONVERTER

In Section II, it has been shown that it is possible to identify the optimal voltage at the dc side of a diode bridge rectifier starting from the measurement of the generator speed. In this section, such result is extended to the case of an active full bridge rectifier, and it is shown how the optimal voltage at the ac side of an active full bridge connected to a regenerative train suspension is related to the generator speed.

Let us consider the equivalent circuit of the electrical subsystem of the regenerative train suspension loaded by a generic load impedance Z , as shown in Fig. 2(b). If the generator speed ω_{gen} is a constant, the induced voltages are purely sinusoidal with angular frequency $n_p \cdot \omega_{gen}$ (see (A.1) in the Appendix) and the internal impedance is $R_{gen} + j \cdot n_p \cdot \omega_{gen} \cdot L_{gen}$ for every generator phase. Hence, the optimal wye connected load impedance, satisfying the maximum power transfer theorem, is the complex conjugate of the internal impedance

$$Z_{OPT} = R_{gen} - j \cdot n_p \cdot \omega_{gen} \cdot L_{gen}. \quad (7)$$

When the generators phases are connected to the wye optimal load given by (7), the optimal line voltages on the load can be written as

$$v_{i_OPT}(t) = V_{OPT} \sin \left(n_p \omega_{gen} t + \delta_{OPT} - \frac{2\pi(i-1)}{3} \right) \quad (8)$$

where

$$V_{OPT} = \frac{k_e \cdot \omega_{gen}}{2 \cdot R_{gen}} \sqrt{R_{gen}^2 + n_p^2 \cdot \omega_{gen}^2 \cdot L_{gen}^2} \quad (9)$$

$$\delta_{OPT} = \text{atan} \left(-\frac{n_p \cdot \omega_{gen} \cdot L_{gen}}{R_{gen}} \right). \quad (10)$$

The results of simulations performed in SPICE environment for a constant generator speed, $\omega_{gen} = 1800$ rpm, and a wye

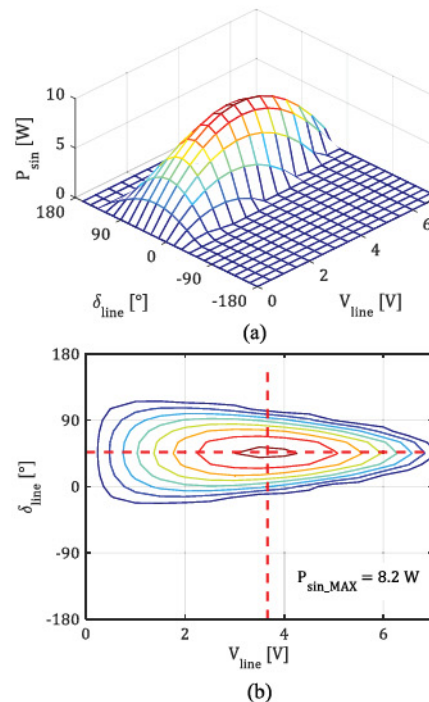


Fig. 5. Results of simulations performed in SPICE environment. (a) Surface of the average extracted power P_{sin} from the considered regenerative train suspension as a function of the amplitude V_{line} and of the phase δ_{line} of the load voltage in presence of a constant generator speed. (b) Corresponding contour plot.

three-phase load voltage, with amplitude V_{line} and phase δ_{line}

$$v_i(t) = V_{line} \sin \left(n_p \omega_{gen} t + \delta_{line} - \frac{2\pi(i-1)}{3} \right) \quad (11)$$

are reported in Fig. 5. In Fig. 5(a), the surface of the average extracted power P_{sin} from the considered regenerative train suspension is reported as a function of the amplitude V_{line} and the phase δ_{line} of the wye connected three-phase load voltages. In Fig. 5(b), the corresponding contour plot is reported. Such results show that there exists a single maximum power point that is equal to the one predicted by (9) and (10) [interception of red dashed lines in Fig. 5(b)].

Let us now consider the equivalent circuit of the electrical subsystem of the regenerative train suspension loaded by an active full bridge rectifier, as shown in Fig. 6(a). In an active full bridge rectifier, the desired amplitude and phase of the fundamental component of the voltage at its input terminals can be imposed by properly controlling its switches. The unipolar six-step pulsewidth modulation (PWM) driving technique is here considered, because it is one of the most widely used for brushless motors [22]–[24]. However, other modulation techniques, like the Sinusoidal PWM, can be used to synthesize a more perfect sinusoidal waveform at the input of the active full bridge rectifier. According to the unipolar six-step PWM driving technique, the switches of the full bridge converter are driven step-by-step, by dividing the electrical cycle $2\pi/(n_p \cdot \omega_{gen})$ into six commutation steps. For each step, one of the generator windings is switched between the dc side voltage $V_{battery}$ and

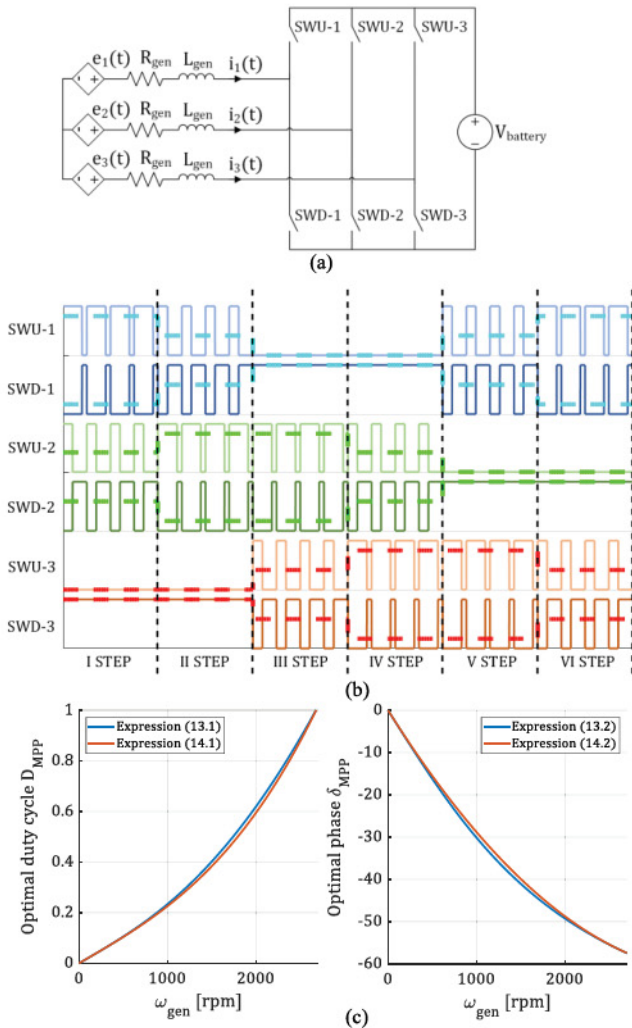


Fig. 6. (a) Equivalent circuit of the regenerative train suspension electrical subsystem loaded by a full bridge rectifier. (b) Example of a switching pattern of the six-step PWM driving technique. Continuous lines represent switches control signals and dashed lines represent duty cycles according to Table II. (c) Optimal duty cycle and phase versus generator speed.

the ground with a duty cycle D , a second winding is connected to ground and a third winding is left open. The successive steps are executed in the same way except that the switched generator phase winding changes to generate a rotating stator field.

Here, the third winding is switched with a duty cycle $0.5 D$, in order to avoid that it remains open, leading to an undefined value for its phase voltage, as shown in Table II and in Fig. 6(b). For this driving technique, it results

$$V_{\text{line}} = \frac{V_{\text{battery}}}{\sqrt{3}} D \Rightarrow D = \sqrt{3} \frac{V_{\text{line}}}{V_{\text{battery}}}. \quad (12)$$

Expression (12) can be used to identify the value of the duty cycle D that ensures a desired amplitude V_{line} of the fundamental component of the voltage at the full bridge input terminals.

TABLE II
SIX-STEP DRIVING TECHNIQUE

	I STEP	II STEP	III STEP	IV STEP	V STEP	VI STEP
SWU-1	D	D_m	0	0	D_m	D
SWD-1	$1-D$	$1-D_m$	1	1	$1-D_m$	$1-D$
SWU-2	D_m	D	D	D_m	0	0
SWD-2	$1-D_m$	$1-D$	$1-D$	$1-D_m$	1	1
SWU-3	0	0	D_m	D	D	D_m
SWD-3	1	1	$1-D_m$	$1-D$	$1-D$	$1-D_m$

D means that the switch is controlled with a duty cycle D ; D_m means that the switch is controlled with a duty cycle $0.5D$; 0 means that the switch is controlled with a duty cycle 0; 1 means that the switch is controlled with a duty cycle 1.

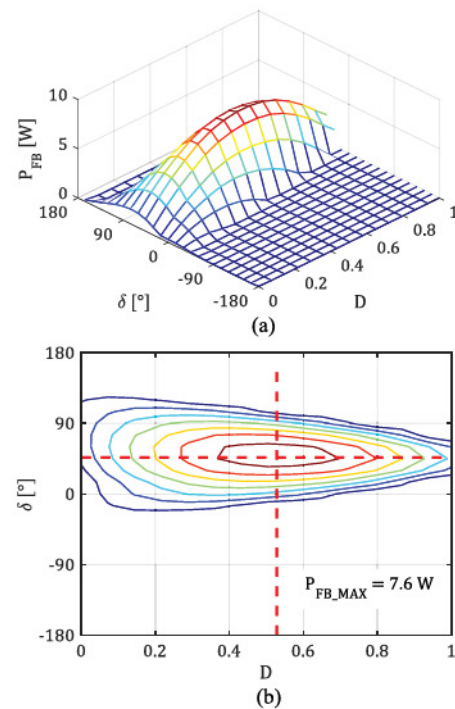


Fig. 7. Results of simulations performed in SPICE environment. (a) Surface of the average extracted power P_{FB} from the considered regenerative train suspension as a function of the amplitude D and of the phase δ of the duty cycle of the full-bridge rectifier in presence of a constant generator speed. (b) Corresponding contour plot.

By exploiting (9), (10), and (12), the optimal duty cycle D_{MPP} and phase δ_{MPP} can be identified for the full-bridge rectifier as

$$\begin{aligned} D_{\text{MPP}} &= \frac{\sqrt{3} \cdot V_{\text{OPT}}}{V_{\text{battery}}} \\ &= \frac{\sqrt{3}}{V_{\text{battery}}} \cdot \frac{k_e \cdot \omega_{\text{gen}}}{2 \cdot R_{\text{gen}}} \sqrt{R_{\text{gen}}^2 + n_p^2 \cdot \omega_{\text{gen}}^2 \cdot L_{\text{gen}}^2} \end{aligned} \quad (13.1)$$

$$\delta_{\text{MPP}} = \delta_{\text{OPT}} = \text{atan} \left(-\frac{n_p \cdot \omega_{\text{gen}} \cdot L_{\text{gen}}}{R_{\text{gen}}} \right). \quad (13.2)$$

The results of simulations performed in SPICE environment are reported in Fig. 7. In particular, in Fig. 7(a), the surface of the average extracted power P_{FB} from the considered regenerative train suspension is reported as a function of the duty cycle D and the phase δ , for a constant generator speed ($\omega_{\text{gen}} = 1800$ rpm).

In Fig. 7(b), the corresponding contour plot is reported. Such results show that there exists a single maximum power point that is equal to the one predicted by (13) [interception of red dashed lines in Fig. 7(b)].

The abovementioned analysis shows that, not only in case of a passive rectifier but also in the case of an active rectifier, it is possible to identify, on the basis of the speed measurement, the optimal operating conditions leading to the maximum power extraction from a regenerative vehicle suspension. It is worth noting that, also in case of an active rectifier, in order to handle the tolerances and time variability of the parameters of the controlled system, a feedback control can be implemented. However, the presence of a feedforward prediction, based on the proposed analysis, can significantly increase the dynamic performance of the whole control system.

In order to simplify the implementation in microcontroller, the converter duty cycle, given by (13), can be approximated as a function of the measured generator speed as

$$D = K_1 \frac{\omega_{gen}}{V_{battery}} [1 + \alpha K_2^2 \omega_{gen}^2] \quad (14.1)$$

$$\delta = -K_2 \omega_{gen} [1 - \beta K_2 \omega_{gen}] \quad (14.2)$$

where $\alpha = 0.35$, $\beta = 0.23$. Starting from (13) it is possible to identify the optimal values of K_1 and K_2 in (14) as

$$K_{1_MPP} = \sqrt{3} \cdot \frac{k_e}{2} \quad K_{2_MPP} = \frac{n_p \cdot L_{gen}}{R_{gen}} \quad (15)$$

In order to validate the approximation, the exact expression (13) and the approximated expression (14) for the optimal duty cycle and phase are reported in Fig. 6(c).

IV. EXPERIMENTAL RESULTS

In this section, experimental results aimed at validating the theoretical analysis presented in the previous sections are shown. In order to carry out laboratory tests, the mechanical part of the regenerative train suspension was emulated by using a dc motor (BLDC58-35L) equipped with a closed-loop speed controller driving the same three-phase generator (Maxon EC-i 40 496652) employed in the actual regenerative train suspension. This setup, as shown in Fig. 8, reproduces the same $\omega_{gen}(t)$ versus $|\omega_{pinion}(t)|$ relation of the considered regenerative train suspension [13].

A. Passive AC–DC Converter – Constant Speed

The first set of experimental tests was carried out in order to validate the theoretical analysis provided in Section II, describing the link between the optimal dc side voltage of a diode bridge rectifier and the generator speed. To this aim, the electromagnetic generator of the considered regenerative train suspension was connected to a three-phase diode bridge rectifier implemented by means of Schottky diodes 1N5817. The diode bridge rectifier was connected to a dc–dc boost converter in order to properly regulate the dc side voltage v_{DC} . A schematic representation of the implemented system is shown in Fig. 9.

In particular, the dc–dc synchronous boost converter was implemented by a $C_{DC} = 100 \mu\text{F}$, an $L_{boost} = 100 \text{ mH}$ and

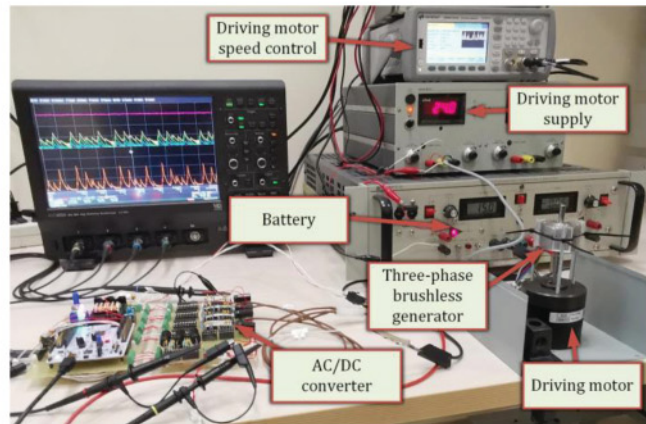


Fig. 8. Experimental setup.

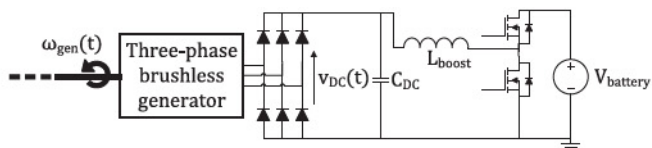


Fig. 9. Schematic representation of the implemented passive ac–dc converter.

the active inverter leg in the L6205 integrated circuit by STMicroelectronics [25]. The switching frequency was set at $f_s = 30 \text{ kHz}$ and the battery voltage at $V_{battery} = 12 \text{ V}$. The generator speed was measured by means of the hall sensors integrated in the considered electromagnetic generator. Moreover, an STM32F401RE microcontroller by STMicroelectronics was used in order to implement the $v_{DC}(t)$ versus $\omega_{gen}(t)$ models described in Section II.

First, constant generator speeds were considered. For each generator speed, the P_{DC} versus v_{DC} characteristic was measured. The obtained measured points and their interpolations are reported in Fig. 10(a).

Fig. 10(b) shows the measured optimal voltages $v_{DC_MPP}(\omega_{gen})$ maximizing the dc power (black curve) and the lines obtained on the basis of the two models shown in Section II. In particular, the red curve refers to the “proportional model” with $m_{MPP} = 3\sqrt{3}/(2\pi) \cdot k_e = 2.3 \text{ mV/rpm}$ and the green curve refers to the “improved model” with $m_{MPP} = 2.3 \text{ mV/rpm}$ and $q_{MPP} = -V_d = -0.3 \text{ V}$. It is possible to observe that even if the “proportional model” is able to identify the optimal voltages with a good approximation, as shown in [13] and [14], the “improved model” is surely a better way for identifying the optimal voltages. This is also confirmed by observing Fig 10(c), where the maximum power points obtained by the two proposed models are placed on the P_{DC} versus v_{DC} curves. It is confirmed that the improved model is able to lead to better power performance.

It is worth noting that, due to the efficiency of the dc–dc stage, the optimal operating point maximizing P_{DC} can be different from the optimal operating point maximizing the power injected into the battery $P_{battery}$. In order to maximize $P_{battery}$, an

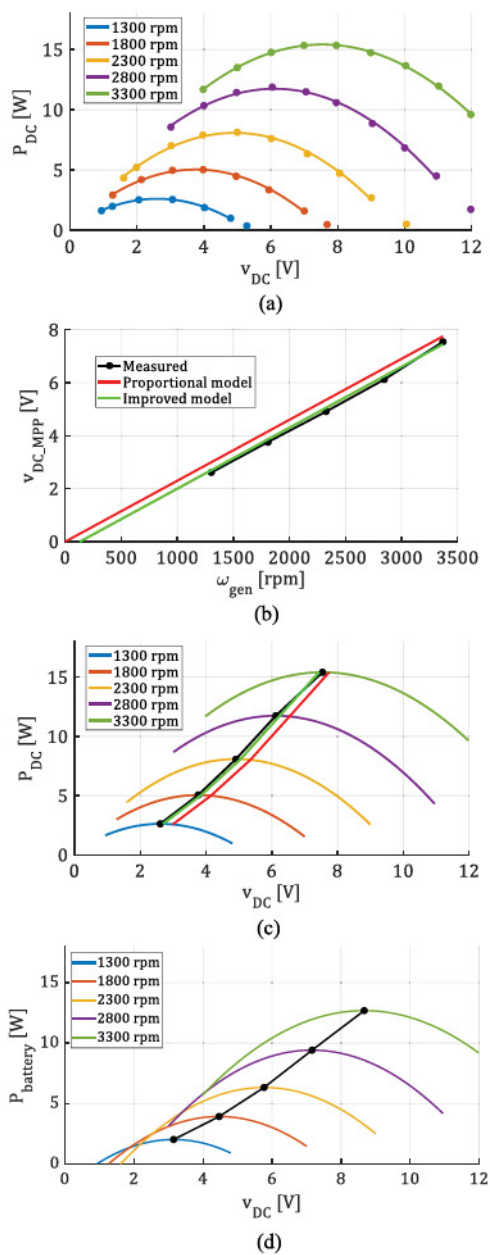


Fig. 10. (a) P_{DC} versus v_{DC} characteristics (measured points and their interpolations) for different ω_{gen} . (b) v_{DC_MPP} versus ω_{gen} measured point and lines obtained with the two considered models. (c) Maximum power points of Fig. 10(b) are placed on the P_{DC} versus v_{DC} interpolated curves. (d) $P_{battery}$ versus v_{DC} characteristics and their maximum power points (black points) for different ω_{gen} .

analytical or experimental model of the dc–dc converter can be included in the feedforward controller or an adaptive control loop can be added, as shown in [14]. In the last case, the proposed P_{DC} versus v_{DC} model can be a very accurate starting point for the adaptive control. Alternatively, it is possible to experimentally characterize the link between $P_{battery}$ and v_{DC} , as it is shown in Fig. 10(d), because also in the case of the battery power maximization, a real-time direct estimation of the maximum power point can be obtained by exploiting the measurement of the generator speed.

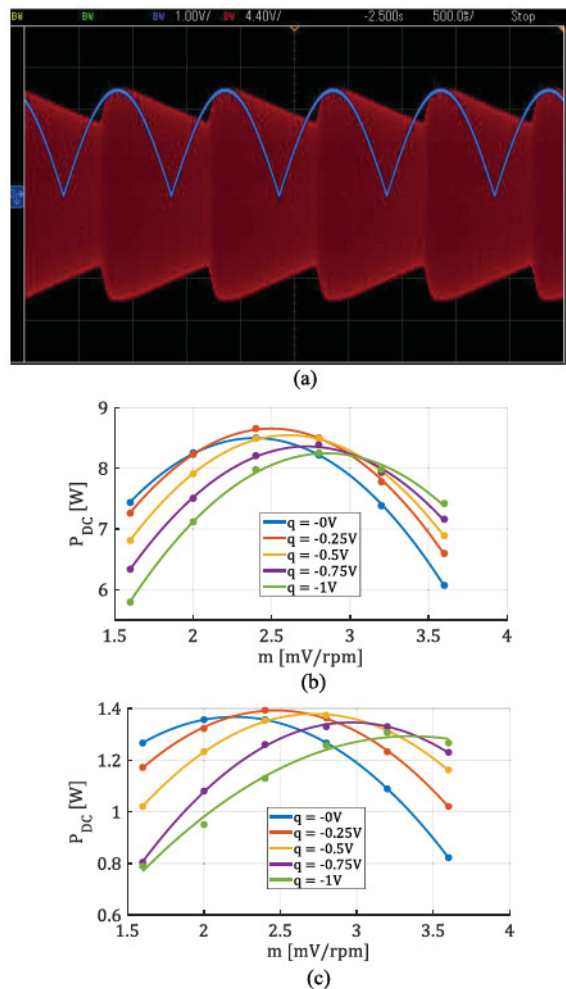


Fig. 11. (a) Oscilloscope screenshot showing the imposed half sinusoidal $|\omega_{pinion}(t)|$ (blue curve) and the line-to-line generator open circuit voltage whose amplitude is proportional to $\omega_{gen}(t)$ (red curve). (b) P_{DC} versus m characteristics (measured points and their interpolations) for different values of q and for ω_{gen_MAX} equal to about 3300 rpm. (c) P_{DC} versus m characteristics for ω_{gen_MAX} equal to about 1300 rpm.

B. Passive AC–DC Converter – Time-Varying Speed

The second set of experimental tests was carried out to show the performance of the proposed $v_{DC_MPP}(\omega_{gen})$ model when the input generator speed is not constant. To this end, the regenerative train suspension was excited by imposing a sinusoidal train suspension vibration leading to a half sinusoidal rectified speed of the pinion shaft $|\omega_{pinion}(t)|$. Such a rectified pinion speed leads to a time-varying generator speed $\omega_{gen}(t)$ according to the engagement/disengagement operation of the MMR described in [13] and [18]. The oscilloscope screenshot reported in Fig. 11(a) shows the trends of the imposed half sinusoidal $|\omega_{pinion}(t)|$ (blue curve) and of the line-to-line open circuit voltage of the electromagnetic generator, whose amplitude is proportional to $\omega_{gen}(t)$ (red curve). The resulting time-varying $\omega_{gen}(t)$ is characterized by a frequency equal to 1 Hz and a peak value ω_{gen_MAX} equal to about 3300 rpm. Fig. 11(b) shows that, in such operating conditions, the extracted power depends on the value of both m and q . In particular, among all the

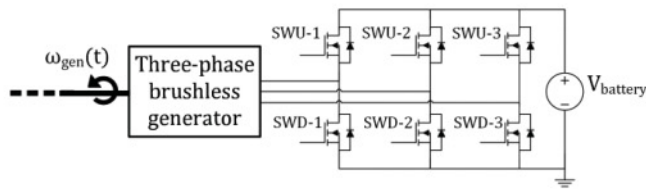


Fig. 12. Schematic representation of the implemented active ac-dc stage.

considered couples (m, q) , the maximum extracted power (peak of the red curve) is obtained in correspondence of the couple $(m = 2.3\text{mV/rpm}, q = -0.25\text{V})$ that is very close to the couple predicted by the improved model ($m_{\text{MPP}} = 3\sqrt{3}/(2\pi) \cdot k_e = 2.3\text{mV/rpm}$ and $q_{\text{MPP}} = -V_d = -0.3\text{V}$).

The considered system was excited also with a half sinusoidal rectified pinion speed $|\omega_{\text{pinion}}(t)|$ leading to a time-varying generator speed $\omega_{\text{gen}}(t)$, with a peak value $\omega_{\text{gen_MAX}}$ equal to about 1300 rpm. The results of these tests are reported in Fig. 11(c) and also in this case show the goodness of the improved model.

Summarizing, expression (6) provides an estimation more accurate than (3) for the optimal voltage at the dc side of a diode bridge rectifier both in case of a constant generator speed and in case of a time-variable generator speed.

C. Active AC-DC Converter – Constant Speed

Experimental tests were carried out also to validate the theoretical analysis provided in Section III, describing the link between the optimal duty cycle of an active full bridge rectifier and the generator speed. To this aim, the electromagnetic generator of the regenerative train suspension was loaded by a three-phase active full bridge rectifier. A schematic representation of the implemented system is shown in Fig. 12.

In particular, the active ac-dc converter was implemented by means of three active rectifier legs in the L6205 DMOS dual full bridge driver integrated circuit by STMicroelectronics [25]. The switching frequency was set at $f_s = 30\text{ kHz}$ and the battery voltage at $V_{\text{battery}} = 12\text{ V}$. The generator speed was measured by means of the hall sensors integrated in the considered electromagnetic generator and the STM32F401RE microcontroller by STMicroelectronics was used in order to implement the unipolar six-step driving PWM modulation and the $d(t)$ versus ω_{gen} model given by (14) and (15).

Also in this case, first constant generator speeds were considered. For each value of the generator speed the average power injected into the battery P_{battery} was measured as a function of the duty cycle D and of the phase δ . In Fig. 13(a), the surface of $P_{\text{battery}}(D, \delta)$ is reported in case of $\omega_{\text{gen}} = 1800\text{ rpm}$. Moreover, in Fig. 13(b), the corresponding contour plot and the optimal amplitude and phase of the duty cycle (interception of red dashed lines), predicted by (13) are reported. Furthermore, in order to simplify the implementation in microcontroller, the converter duty cycle was calculated by means of (14), as a function of K_1 and K_2 . The average power injected into the battery P_{battery} was measured as a function of K_1 and K_2 and is reported in Fig. 14.

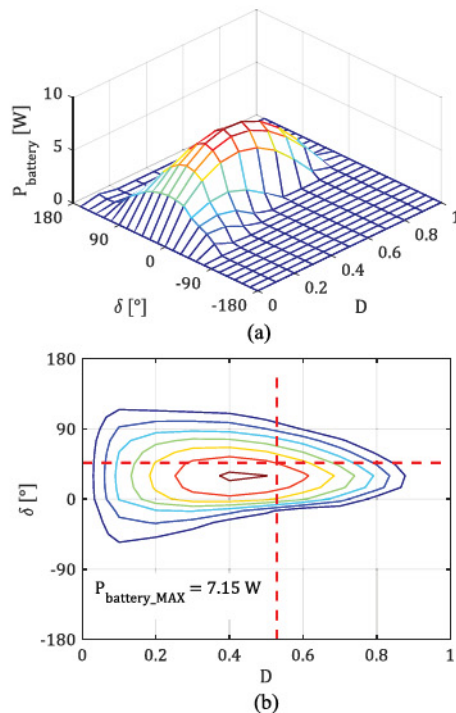


Fig. 13. Experimental results. (a) Surface of the average extracted power P_{battery} from the considered regenerative train suspension measured in case of $\omega_{\text{gen}} = 1800\text{ rpm}$, as a function of the amplitude D and of the phase δ of the duty cycle of the full-bridge rectifier. (b) Corresponding contour plot.

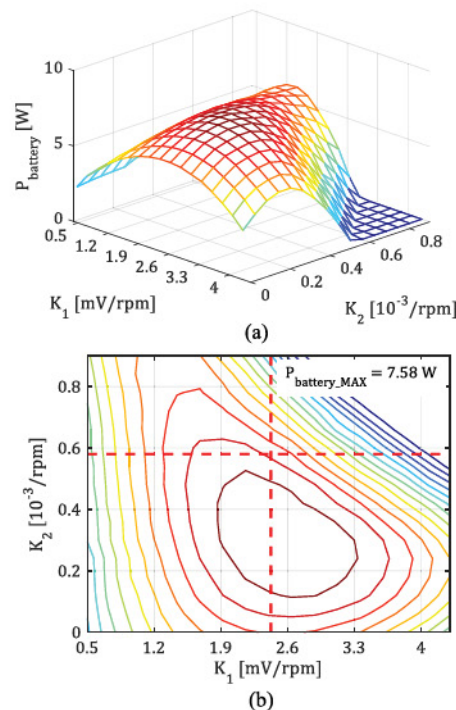


Fig. 14. Experimental results. (a) Surface of the average extracted power P_{battery} from the considered regenerative train suspension measured in case of $\omega_{\text{gen}} = 1800\text{ rpm}$, as a function of K_1 and K_2 . (b) Corresponding contour plot.

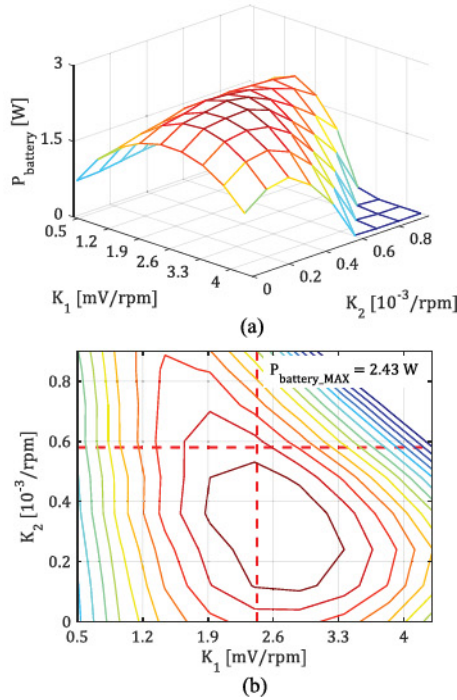


Fig. 15. Experimental results. (a) Surface of the average extracted power P_{battery} from the considered regenerative train suspension, as a function of K_1 and K_2 , measured in case that $\omega_{\text{gen}}(t)$ has a half sinusoidal shape with $\omega_{\text{gen_MAX}} = 1800$ rpm. (b) Corresponding contour plot.

Figs. 13 and 14 confirm that the system is characterized by a single maximum power point for which a good first order approximation can be provided by expressions (13) and (15), respectively. The discrepancies in the identification of the maximum power points, which are mainly due to the switches' losses neglected in the proposed analysis, can be reduced by an adaptive control loop.

D. Active AC–DC Converter – Time-Varying Speed

The second set of experimental tests with the active ac–dc converter was carried out to show the system behavior when the input generator speed is not a constant. The regenerative train suspension loaded by the full-bridge rectifier was excited with a half sinusoidal rectified speed of the pinion shaft $|\omega_{\text{pinion}}(t)|$ with frequency 1 Hz, like the one shown in Fig. 11(a), corresponding to a sinusoidal train suspension vibration. Such a pinion speed leads to a time-varying generator speed $\omega_{\text{gen}}(t)$, with a peak value $\omega_{\text{gen_MAX}}$ equal to about 1800 rpm [13], [18]. The average power injected into the battery P_{battery} was measured as a function of K_1 and K_2 and is reported in Fig. 15.

Such results show that also in the case of an active full-bridge rectifier, it is possible to identify the optimal operating conditions leading to the maximum power extraction from a regenerative train suspension, on the basis of the measurement of the generator speed $\omega_{\text{gen}}(t)$.

V. CONCLUSION

This article dealt with ac–dc converters for regenerative train suspensions. For the first considered ac–dc converter, a diode

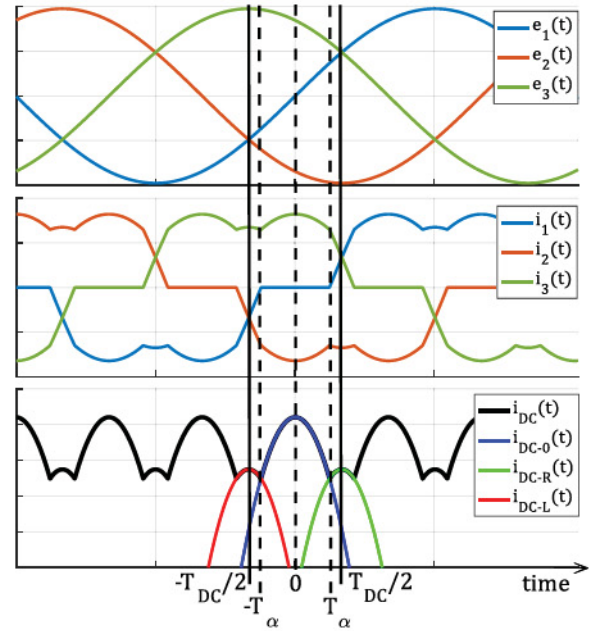


Fig. 16. Typical trends of the ac phase voltages, of the ac phase currents and of the dc current as obtained by a SPICE simulation.

bridge rectifier, it has been theoretically and experimentally shown that the optimal value of the dc side voltage can be predicted starting from the measurement of the generator speed. A speed-voltage model has been proposed that is very accurate not only in case of ideal constant generator speeds, but also in case of more realistic time-variable generator speeds. The second considered ac–dc converter is an active full-bridge rectifier. It has been theoretically and experimentally shown that, also in this case, a relationship exists between the optimal converter duty cycle and the generator speed. The models proposed in this article can be effectively exploited for designing high-performance maximum power point tracking techniques for ac–dc rectifiers in regenerative train suspensions applications.

APPENDIX

When the generator speed ω_{gen} is a constant, the induced voltages, e_1 , e_2 , and e_3 , are purely sinusoidal and can be written as

$$e_i(t) = k_e \cdot \omega_{\text{gen}} \cdot \sin\left(n_p \cdot \omega_{\text{gen}} \cdot t - \frac{2\pi(i-1)}{3}\right) \quad (\text{A.1})$$

where $i = 1, 2, 3$ is the number of the generator's phase.

By neglecting the generator's phase coils inductance L_{gen} and the diodes voltage drops V_d , the current in the dc side is a periodic waveform, with a period $T_{\text{DC}} = \pi/(3 \cdot n_p \cdot \omega_{\text{gen}})$.

In particular, according to the circuit schematic shown in Fig. 3, for t around zero only phases 2 and 3 conduct current, because e_1 is not high enough to switch on the diodes connected to the phase 1, as it is shown in Fig. 16. Hence, for $t \in [-T_{\alpha}, T_{\alpha}]$,

the dc side current can be written as

$$i_{\text{DC}-0}(t) = \frac{e_3 - e_2 - v_{\text{DC}}}{2 \cdot R_{\text{gen}}} = \frac{\sqrt{3}k_e\omega_{\text{gen}} \cos(n_p\omega_{\text{gen}}t) - v_{\text{DC}}}{2 \cdot R_{\text{gen}}} \quad (\text{A.2})$$

The abovementioned condition holds until, at $t = T_\alpha$, e_1 becomes equal to the positive potential of v_{DC} and, thus, it is high enough to switch on the upper diode connected to phase 1. Thus, at $t = T_\alpha$, it holds the equation

$$e_1(T_\alpha) = e_3(T_\alpha) - R_{\text{gen}} \cdot i_{\text{DC}-0}(T_\alpha) \quad (\text{A.3})$$

which can be exploited to predict the value of T_α , starting from (A.1) and (A.2)

$$T_\alpha = \frac{a \sin\left(\frac{v_{\text{DC}}}{3k_e\omega_{\text{gen}}}\right)}{n_p\omega_{\text{gen}}} \quad (\text{A.4})$$

For $t \in [T_\alpha, T_{\text{DC}}/2]$, all the three generator phases conduct and, by applying the superposition principle, the dc side current can be written as

$$\begin{aligned} i_{\text{DC}-R}(t) &= -\frac{e_2}{R_{\text{gen}}} - \frac{2v_{\text{DC}}}{3R_{\text{gen}}} \\ &= \frac{-k_e\omega_{\text{gen}} \sin(n_p\omega_{\text{gen}}t - \frac{2\pi}{3})}{R_{\text{gen}}} - \frac{2v_{\text{DC}}}{3R_{\text{gen}}} \end{aligned} \quad (\text{A.5})$$

Similarly, also for $t \in [-T_{\text{DC}}/2, -T_\alpha]$, the dc side current is

$$i_{\text{DC}-L}(t) = \frac{k_e\omega_{\text{gen}} \sin(n_p\omega_{\text{gen}} \cdot t + \frac{2\pi}{3})}{R_{\text{gen}}} - \frac{2v_{\text{DC}}}{3R_{\text{gen}}} \quad (\text{A.6})$$

Therefore, the instantaneous extracted power can be written as

$$p_{\text{DC}}(t) = \begin{cases} v_{\text{DC}} \cdot i_{\text{DC}-L}(t) & \forall t \in [-\frac{T_{\text{DC}}}{2}, -T_\alpha] \\ v_{\text{DC}} \cdot i_{\text{DC}-0}(t) & \forall t \in [-T_\alpha, T_\alpha] \\ v_{\text{DC}} \cdot i_{\text{DC}-R}(t) & \forall t \in [T_\alpha, \frac{T_{\text{DC}}}{2}] \end{cases} \quad (\text{A.7})$$

By averaging (A.7), the mean extracted power P_{DC} can be obtained

$$P_{\text{DC}} = P_{\text{DC}-0} + P_{\text{DC}-L} + P_{\text{DC}-R} \quad (\text{A.8})$$

where

$$\begin{aligned} P_{\text{DC}-0} &= \frac{v_{\text{DC}}}{T_{\text{DC}}} \int_{-T_\alpha}^{T_\alpha} \frac{\sqrt{3}k_e\omega_{\text{gen}} \cos(n_p\omega_{\text{gen}} \cdot t)}{2 \cdot R_{\text{gen}}} dt \\ &\quad - \frac{1}{T_{\text{DC}}} \int_{-T_\alpha}^{T_\alpha} \frac{v_{\text{DC}}^2}{2 \cdot R_{\text{gen}}} dt \end{aligned} \quad (\text{A.9})$$

and

$$\begin{aligned} P_{\text{DC}-L} = P_{\text{DC}-R} &= -\frac{1}{T_{\text{DC}}} \int_{-\frac{T_{\text{DC}}}{2}}^{-T_\alpha} \frac{2v_{\text{DC}}^2}{3R_{\text{gen}}} dt \\ &\quad + \frac{v_{\text{DC}}}{T_{\text{DC}}} \int_{-\frac{T_{\text{DC}}}{2}}^{-T_\alpha} \frac{k_e\omega_{\text{gen}} \sin(n_p\omega_{\text{gen}}t + \frac{2\pi}{3})}{R_{\text{gen}}} dt. \end{aligned} \quad (\text{A.10})$$

By solving (A.9), it results

$$P_{\text{DC}-0} = \frac{v_{\text{DC}}}{T_{\text{DC}}} \frac{\sqrt{3}k_e}{R_{\text{gen}}n_p} \sin(n_p\omega_{\text{gen}} \cdot T_\alpha) - \frac{T_\alpha}{T_{\text{DC}}} \frac{v_{\text{DC}}^2}{R_{\text{gen}}} \quad (\text{A.11})$$

By solving (A.10), it results

$$\begin{aligned} P_{\text{DC}-L} = P_{\text{DC}-R} &= -\frac{T_{\text{DC}} - 2T_\alpha}{T_{\text{DC}}} \cdot \frac{v_{\text{DC}}^2}{3R_{\text{gen}}} \\ &\quad - \frac{v_{\text{DC}}}{T_{\text{DC}}} \frac{k_e}{n_p R_{\text{gen}}} \cos\left(n_p\omega_{\text{gen}}T_\alpha - \frac{2\pi}{3}\right). \end{aligned} \quad (\text{A.12})$$

Hence, (A.8) can be written as

$$P_{\text{DC}} = \frac{v_{\text{DC}}^2}{R_{\text{gen}}} \left[\frac{T_\alpha - 2T_{\text{DC}}}{3T_{\text{DC}}} \right] + \frac{v_{\text{DC}}}{T_{\text{DC}}} \frac{k_e \cos(n_p\omega_{\text{gen}}T_\alpha)}{n_p R_{\text{gen}}} \quad (\text{A.13})$$

In order to find the optimal value $v_{\text{DC_MPP}}$ of v_{DC} that maximizes P_{DC} , (A.13) should be differentiated with respect to v_{DC} and the result should be equated to zero. Unfortunately, a closed form expression of $v_{\text{DC_MPP}}$ cannot be obtained, due to the presence of the $\text{asin}(\cdot)$ function in (A.4). However, a first order approximation of the expression of $v_{\text{DC_MPP}}$ can be obtained in closed form for $T_\alpha \rightarrow T_{\text{DC}}/2$, leading to a small error in practical applications, as it was shown in [14]. For $T_\alpha \rightarrow T_{\text{DC}}/2$, according to (A.7), the instantaneous power $p_{\text{DC}}(t) \rightarrow v_{\text{DC}} \cdot i_{\text{DC}-0}(t)$ for $t \in [-T_{\text{DC}}/2, T_{\text{DC}}/2]$ and, hence, can be written as in (1).

REFERENCES

- [1] L. Li, Y. Zhang, C. Yang, B. Yan, and C. M. Martinez, "Model predictive control-based efficient energy recovery control strategy for regenerative braking system of hybrid electric bus," *Energy Convers. Manage.*, vol. 111, no. 1, pp. 299–314, Mar. 2016.
- [2] M. Balato, L. Costanzo, and M. Vitelli, "MPPT in wireless sensor nodes supply systems based on electromagnetic vibration harvesters for freight wagons applications," *IEEE Trans. Ind. Electron.*, vol. 64, no. 5, pp. 3576–3586, May 2017.
- [3] Y. Zhang, K. Guo, D. Wang, C. Chen, and X. Li, "Energy conversion mechanism and regenerative potential of vehicle suspensions," *Energy*, vol. 119, pp. 961–970, Jan. 2017.
- [4] M. A. A. Abdelkareem *et al.*, "Vibration energy harvesting in automotive suspension system: A detailed review," *Appl. Energy*, vol. 229, pp. 672–699, 2018.
- [5] J. Dicken, P. D. Mitcheson, I. Stoianov, and E. M. Yeatman, "Power-extraction circuits for piezoelectric energy harvesters in miniature and low-power applications," *IEEE Trans. Power Electron.*, vol. 27, no. 11, pp. 4514–4529, Nov. 2012.
- [6] L. Costanzo, A. Lo Schiavo, and M. Vitelli, "Power extracted from piezoelectric harvesters driven by non-sinusoidal vibrations," *IEEE Trans. Circ. Sys. I, Regular Papers*, vol. 66, no. 3, pp. 1291–1303, Mar. 2019.
- [7] M. Balato, L. Costanzo, and M. Vitelli, "Maximization of the extracted power in resonant electromagnetic vibration harvesters applications employing bridge rectifiers," *Sensors Actuators A, Phys.*, vol. 263, pp. 63–75, 2017. [Online]. Available: <https://doi.org/10.1016/j.sna.2017.04.002>
- [8] L. Costanzo, A. Lo Schiavo, and M. Vitelli, "Power maximization from resonant electromagnetic vibration harvesters feeding bridge rectifiers," *Int. J. Circuit Theor. Appl.*, vol. 47, no. 1, pp. 87–102, Jan. 2019.
- [9] K. H. Tse and H. S. Chung, "MPPT for electromagnetic energy harvesters having nonnegligible output reactance operating under slow-varying conditions," *IEEE Trans. Power Electron.*, vol. 35, no. 7, pp. 7110–7122, Jul. 2020, doi: [10.1109/TPEL.2019.2959625](https://doi.org/10.1109/TPEL.2019.2959625).
- [10] M. Carandell, D. M. Toma, M. Carbonell, J. del Rio, and M. Gasulla, "Design and testing of a kinetic energy harvester embedded into an oceanic drifter," *IEEE Sensors J.*, vol. 20, no. 23, pp. 13930–13939, Dec. 2020, doi: [10.1109/JSEN.2020.2976517](https://doi.org/10.1109/JSEN.2020.2976517).

- [11] L. Costanzo, A. L. Schiavo, and M. Vitelli, "Design guidelines for the perturb and observe technique for electromagnetic vibration energy harvesters feeding bridge rectifiers," *IEEE Trans. Ind. Appl.*, vol. 55, no. 5, pp. 5089–5098, Sep./Oct. 2019.
- [12] L. Costanzo, M. Vitelli, Y. Pan, and L. Zuo, "Maximizing the power extraction from train suspension energy harvesting system," in *Proc. Int. Des. Eng. Tech. Conf. Comp. Inf. Eng. Conf.*, vol. 8, Aug. 2019, pp. 1–7.
- [13] L. Costanzo, M. Vitelli, A. Lo Schiavo, and L. Zuo, "Optimization of diode bridge rectifier output voltage in train suspension energy harvesters," in *Proc. IEEE 20th Mediterranean Electrotechnical Conf.*, Palermo, Italy, 2020, pp. 197–201, doi: [10.1109/MELECON48756.2020.9140723](https://doi.org/10.1109/MELECON48756.2020.9140723).
- [14] L. Costanzo, T. Lin, W. Lin, A. Lo Schiavo, M. Vitelli, and L. Zuo, "Power electronic interface with an adaptive MPPT technique for train suspension energy harvesters," in *IEEE Trans. Ind. Electron.*, vol. 68, no. 9, pp. 8219–8230, Sep. 2021, doi: [10.1109/TIE.2020.3009584](https://doi.org/10.1109/TIE.2020.3009584).
- [15] S. F. Toloue and M. Moallem, "Multivariable sliding-mode extremum seeking control with application to MPPT of an alternator-based energy conversion system," *IEEE Trans. Ind. Electron.*, vol. 64, no. 8, pp. 6383–6391, Aug. 2017.
- [16] H. K. Seyed, M. Mehrdad, and A. Siamak, "A two-variable extremum seeking controller with application to self-tuned vibration energy harvesting," *Smart Mater. Structures*, vol. 28, no. 9, 2019, Art. no. 095027, doi: [10.1088/1361-665X/ab028b](https://doi.org/10.1088/1361-665X/ab028b).
- [17] L. Costanzo, A. Lo Schiavo, and M. Vitelli, "Active interface for piezoelectric harvesters based on multi-variable maximum power point tracking," *IEEE Trans. Circuits Syst. I: Regular Papers*, vol. 67, no. 7, pp. 2503–2515, Jul. 2020, doi: [10.1109/TCSL.2020.2977495](https://doi.org/10.1109/TCSL.2020.2977495).
- [18] Y. Pan, F. Liu, R. Jiang, Z. Tu, and L. Zuo, "Modeling and onboard test of an electromagnetic energy harvester for railway cars," *Appl. Energy*, vol. 250, no. 5, pp. 568–581, 2019.
- [19] L. Costanzo, A. L. Schiavo, M. Vitelli, and L. Zuo, "Train suspension energy harvesting system maximizing the output DC power," in *Proc. IEEE Int. Symp. Circuits Syst.*, Sevilla, Spain, 2020, pp. 1–5, doi: [10.1109/IS-CAS45731.2020.9180968](https://doi.org/10.1109/IS-CAS45731.2020.9180968).
- [20] Y. Pan, F. Liu, R. Jiang, Z. Tu, and L. Zuo, "Design, modeling and lab test of electromagnetic energy harvester for railway vehicle suspensions," in *Proceedings of the ASME 2017 International Design Engineering Technical Conferences and Computers and Information in Engineering Conference*, vol. 3, Cleveland, OH, USA, Aug. 2017, pp. 1–9, Paper V003T01A018. [Online]. Available: <https://doi.org/10.1115/DETC2017-67885>
- [21] Model EC-i 40, number 496652 specifications, Maxon. Accessed: Sep. 2021. [Online]. Available: <https://www.maxongroup.com/maxon/view/product/496652>
- [22] UM2124 User manual, *STMicroelectronics*. Accessed: Mar. 29, 2021. [Online]. Available: https://www.st.com/resource/en/user_manual/dm00334922-getting-started-with-the-sixstep-firmware-library-for-stm32-nucleo-boards-based-on-stm32f-microcontrollers-stmicroelectronics.pdf
- [23] Trapezoidal control of BLDC motors using hall effect sensors, texas instruments. Accessed: Mar. 29, 2021. [Online]. Available: https://www.ti.com/lit/an/sprabz4/sprabz4.pdf?ts=1617029531813&ref_url=https%25A%252F%252Fwww.google.com%252F
- [24] Brushless DC motor control made easy, microchip. Accessed: Mar. 29, 2021. [Online]. Available: <http://ww1.microchip.com/downloads/en/appnotes/00857b.pdf>
- [25] L6205 DMOS dual full bridge driver datasheet, *STMicroelectronics*. Accessed: Sep. 9, 2021. [Online]. Available: <https://www.st.com/resource/en/datasheet/l6205.pdf>



Luigi Costanzo was born in Italy, in 1989. He received the master's degree (*cum laude*) in electronic engineering from the Second University of Naples, Naples, Italy, in 2014, and the Ph.D. degree in industrial and information engineering from the Department of Industrial and Information Engineering, Università degli Studi della Campania "Luigi Vanvitelli," Caserta, Italy, in 2017.

He is currently a Research Fellow with the Department of Engineering, Università degli Studi della Campania "Luigi Vanvitelli." His main research interests include maximum power point tracking techniques in photovoltaic applications, power electronics circuits for renewable energy sources, and methods for analysis, design, and optimization of energy harvesting systems.



Alessandro Lo Schiavo (Senior Member, IEEE) was born in Naples, Italy, in 1972. He received the Laurea degree (*cum laude*) in electronic engineering from the Università degli Studi di Napoli, Naples, Italy, in 1997, and the Ph.D. degree in electrical energy conversion from the Seconda Università degli Studi di Napoli, Naples, Italy, in 2000.

From 2001 to 2017, he was Assistant Professor with the Dipartimento di Ingegneria dell'Informazione, Seconda Università degli Studi di Napoli, Italy. Since 2017, he has been an Associate Professor of Electronics with the Università degli Studi della Campania "Luigi Vanvitelli," Italy, where he teaches fundamentals of microelectronics and design of electronic circuits. His current research interests include the areas of electronic circuits for energy harvesting, wireless sensor networks, analysis and design of analog circuits, and nonlinear circuit theory.

Prof. Schiavo is an Associate Editor of the *International Journal of Circuit Theory and Applications*, and of the *Mathematical Problems in Engineering Journal*.

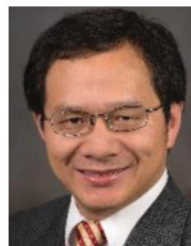


Massimo Vitelli was born in Caserta, Italy, in 1967. He received the laurea degree (*cum laude*) in electrical engineering from the University of Naples Federico II, Naples, Italy, in 1992.

He is currently a Full Professor with the Department of Engineering, Università degli Studi della Campania "Luigi Vanvitelli," where he teaches electric circuits and power electronics. He is engaged in many scientific national projects. He has coauthored a number of national and international patents and two scientific books. His main research interests include

maximum power point tracking techniques in photovoltaic applications, power electronics circuits for renewable energy sources, and methods for analysis, design and optimization energy harvesting systems.

Prof. Vitelli is an Associate Editor for the *IEEE TRANSACTIONS ON POWER ELECTRONICS*.



Lei Zuo received the B.S. degree in automotive engineering from Tsinghua University, Beijing, China, in 1997, and the M.S. degree in mechanical and electrical engineering and the Ph.D. degree in mechanical engineering from the Massachusetts Institute of Technology, Cambridge, MA, USA, in 2002 and 2005, respectively.

He is the Robert E. Hord Jr. Professor with Virginia Tech, Blacksburg, VA, USA, and the Director of the NSF Industry-University Cooperative Research Center for Energy Harvesting Materials and Systems.

He has authored more than 340 research papers and has advised 16 Ph.D. and 50 master's to completion of their degrees. His research interests include design, dynamics, control, and manufacturing of energy systems, with applications to marine energy conversion, vibration energy harvesting, and self-powered control and sensing.

Prof. Zuo was the sole recipient of the 2017 ASME Leonardo Da Vinci Award and the 2015 ASME Thar Energy Design Award. He also won two R&D 100 Awards by R&D Magazine in 2015 and 2011, and Ralph R. Teetor Educational Award by SAE in 2014. He is a Fellow of ASME.